# Experimental study on pore connectivity and its influence on chloride transport in saturated cementitious system

Zhang, Yong; Ye, Guang

**Publication date**
2016

**Document Version**
Accepted author manuscript

**Published in**
Proceedings of the 3rd International RILEM Conferences on Microstructure Related Durability of Cementitious Composites

**Citation (APA)**
Zhang, Y., & Ye, G. (2016). Experimental study on pore connectivity and its influence on chloride transport in saturated cementitious system. In C. Miao, W. Sun, J. Liu, H. Chen, G. Ye, & K. van Breugel (Eds.), *Proceedings of the 3rd International RILEM Conferences on Microstructure Related Durability of Cementitious Composites: Nanjing, China* (Vol. 117, pp. 1-8). Rilem.

**Important note**
To cite this publication, please use the final published version (if applicable).
Please check the document version above.

# Experimental study on pore connectivity and its influence on chloride transport in saturated cementitious system

**Yong Zhang (1), Guang Ye (1)**

(1) Microlab, Delft University of Technology, Netherlands.

## Abstract

The purpose of this paper is to investigate the pore connectivity and its influence on chloride transport property in cementitious materials under saturated condition. Mercury intrusion porosimetry experiment was carried out on a variety of hydrated cement pastes curing up to one year. By repeating pressurization-depressurization cycles, pore entrapment (namely ink-bottled effect) was expressed as a function of the equivalent diameter of penetrated throat neck pores. Accordingly, the small capillary pores that are present within patches of hydration products and the large capillary pores that are left out of hydration products were distinguished and their connections were ascertained, which provide evident basis for the study of transport property estimated by means of rapid chloride migration test on mortar samples. The results suggested that in hydrated cementitious system the capillary pore connections influencing mass transport should be mainly attributed to the connectivity of small capillary pores, whose relevance to chloride migration coefficient has also been testified by the well-fitted experimental plots in this study.

*Key words*: cementitious system, microstructure, pore connectivity, chloride transport

## 1. INTRODUCTION

Microstructure related properties have been widely studied in modern concrete science. Pore structure is one microstructural indicator that highly affects mass transport in concrete [1]. Capillary transport is a main concern for mass penetration [2]. According to refinement mechanism, two types of capillary pores (10nm~10μm) have been distinguished in hardened cement matrix [3]: small capillary pores that refer to void space due to insufficient packing of hydration products and large capillary pores that represent void space left out of hydration products. When cement grains react with water, the hydration products are created and precipitated in originally water-filled space. Each cement grain is growing outwards until contact with neighbouring cement grain (Figure 1a), initiating so called contact area [4] as marked in hydration cell (Figure 1b). The contact area is enlarged with continuous hydration.

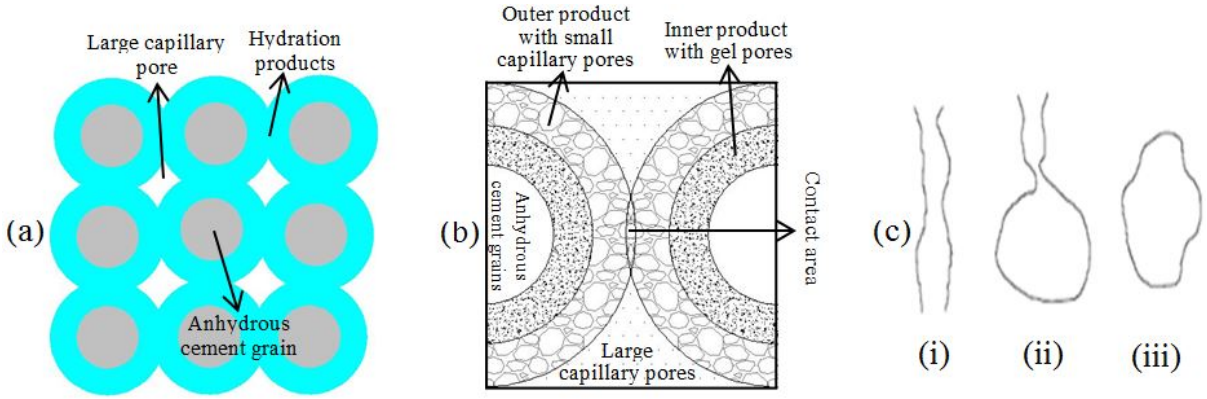


Figure 1: (a) Sketch of hydrated microstructure; (b) hydration cell of two cement grains; (c) pore geometry for continuous pore (i) and dead-end pore (ii) and isolated pore (iii).

The percolation theory [5] has been long time applied to explain mass transport in porous cementitious materials, in which the mass transport is primarily illustrated against the connectivity of capillary pores. In hydrated cement paste, capillary pores with different dimensions are mutually connected with varying pore geometries. A typical classification of the pore geometries can be illustrated in Figure 1c [6]: (i) continuous pores, refer to those can make up an interconnected network relating the two opposite surfaces of a paste specimen; (ii) dead-end pores, which are connected with only one surface of a paste specimen; (iii) isolated pores, which are surrounded by solid phases and have no connection with any surface of a paste specimen. The isolated pores have no impact on mass transport; therefore they are not of interest in usual pore structure analysis. Both the continuous pores and dead-end pores are interconnected in the porous channels and contribute to the total capillary porosity. While it should be noted that the continuous pores predominantly control the mass transport.

Previously, pore connection in cementitious materials was often studied through simulated work [6], yet very limited experimental data has been obtained. Mercury intrusion porosimetry (MIP) is a useful technique in characterizing pore structure of cementitious materials. Through standard MIP test, pore structure parameters, such as total porosity and threshold pore diameter, have been well-documented [7]. However, current standard MIP test has rarely been used to describe the details of pore connections in cementitious materials. Note that mercury intrusion measures the pore size based on the accessible throat neck (i.e.

continuous pores) to reach internal pores (i.e. dead-end pores). With the assumption that dead-end pores remain filled with entrapped mercury after completion of the 1st mercury intrusion-extrusion cycle, no remaining mercury is expected when performing the 2nd cycle. Accordingly, if additional extrusion-intrusion cycles are applied, the both continuous pores and dead-end pores can be determined through mercury penetration measurement.

This work attempts to experimentally investigate the pore connection and its influence on chloride transport in saturated cementitious materials. Mercury penetration experiment with additional extrusion-intrusion cycles was carried out on hydrated paste specimens made of varying cement types curing up to 375 days. Various water-binder ratios (0.4, 0.5 and 0.6) and different blends (fly ash, ground granulated blast furnace slag and limestone powder) were considered in specimen preparation. The results provide direct evidence for studying the mass transport in mortar specimens as indicated by rapid chloride migration test. The effect of pore structure, in particular pore connectivity, on mass transport is determined eventually.

## 2. EXPERIMENTAL PROGRAM

### 2.1 Materials and samples

Raw materials used in this work are ordinary Portland cement (CEM I 42.5N), low-calcium fly ash (FA), ground granulated blast furnace slag (GGBFS) and limestone powder (LP). Cement paste and mortar samples were cast, with both made with the same binder. The binder mixtures include pure OPC, binary and ternary cements. Mix proportions of the binders are given in table 1.

Table 1: Mix proportions and substitutions by mass of binder

| Binder mixtures | OPC | GGBFS | FA | LP | w/b |
|---|---|---|---|---|---|
| P4 | 100% | - | - | - | 0.4 |
| P5 | 100% | - | - | - | 0.5 |
| P6 | 100% | - | - | - | 0.6 |
| PB4 | 30% | 70% | - | - | 0.4 |
| PB5 | 30% | 70% | - | - | 0.5 |
| PB6 | 30% | 70% | - | - | 0.6 |
| PF5 | 70% | - | 30% | - | 0.5 |
| PFL5 | 65% | - | 30% | 5% | 0.5 |

### 2.2 Pore structure measurement

Mercury intrusion experiment was conducted following a unique procedure, which contains one low pressure intrusion step (0-0.17 MPa) and twenty high pressure intrusion steps. The maximum applied pressure at each high pressure intrusion step is indicated in table 2. Note that each high pressure intrusion step is followed by an extrusion procedure (with minimum extruded pressure to 0.17 MPa). Herein the intrusion step 20 is in fact the 2nd intrusion branch of mercury intrusion. With the assumption that pores are cylindrical and entirely and equally accessible to mercury, the correlation between the applied pressure and the pore diameter can be described using the Washburn equation [8]:

$$D=(-4\gamma\cos\theta)/P \quad (1)$$

where, D is the equivalent pore diameter being entered, P is the pressure required to overcome the opposition to entry (max. 210 MPa in this work), $\gamma$ is the surface tension of mercury (0.484 N/m), $\theta$ is the contact angle between mercury and pore wall (138 º).

Table 2: Intrusion steps, maximum applied pressures and minimum intruded pore diameters

| Intrusion Steps *i* | Applied pressure $P_i$ [MPa] (Pore diameter $d_i$ [nm]) | Intrusion Steps *i* | Applied pressure $P_i$ [MPa] (Pore diameter $d_i$ [nm]) |
|---|---|---|---|
| 1 | 0.17 (8200) – 3.40 (423) | 11 | 0.17 (8200) – 77.66 (18.6) |
| 2 | 0.17 (8200) – 5.56 (259) | 12 | 0.17 (8200) – 95.74 (15.1) |
| 3 | 0.17 (8200) – 10.39 (139) | 13 | 0.17 (8200) – 109.88 (13.1) |
| 4 | 0.17 (8200) – 15.82 (91) | 14 | 0.17 (8200) – 117.79 (12.2) |
| 5 | 0.17 (8200) – 20.77 (69.4) | 15 | 0.17 (8200) – 126.25 (11.4) |
| 6 | 0.17 (8200) – 25.56 (56.4) | 16 | 0.17 (8200) – 135.42 (10.6) |
| 7 | 0.17 (8200) – 31.47 (45.8) | 17 | 0.17 (8200) – 166.76 (8.6) |
| 8 | 0.17 (8200) – 33.86 (42.6) | 18 | 0.17 (8200) – 178.71 (8.1) |
| 9 | 0.17 (8200) – 41.61 (34.6) | 19 | 0.17 (8200) – 210.00 (7.0) |
| 10 | 0.17 (8200) – 58.9 (24.5) | 20 | 0.17 (8200) – 210.00 (7.0) |

At each intrusion step, mercury penetrates into microstructure through throat neck pores (i.e. continuous pores) to reach the internal pores (i.e. dead-end pores). At intrusion step *i-1 (i)*, the minimum diameter of intruded continuous pores is $d_{i-1}$ $(d_i)$, the cumulative intruded volume is $V_{i-1}^{in}$ $(V_i^{in})$ and the subsequent cumulative extruded volume is $V_{i-1}^{ex}$ $(V_i^{ex})$. From intrusion step *i-1* to *i*, the incremental volume of intruded pores is $\Delta_i^{in}$ $(\Delta_i^{in} = V_i^{in} - V_{i-1}^{in})$ and the incremental volume of extruded pores is $\Delta_i^{ex}$ $(\Delta_i^{ex} = V_i^{ex} - V_{i-1}^{ex})$. $\Delta_i^{ex}$ and $(\Delta_i^{in} - \Delta_i^{ex})$ can be considered as the volume of continuous pores and dead-end pores after completion of mercury intrusion through throat neck pores at diameter $d_i$. Herein the pore entrapment $\alpha_{en}$ is introduced to quantify the connection of pores at diameter $d_i$, it is calculated as the ratio of entrapped volume over the intruded volume, as $(\Delta_i^{in} - \Delta_i^{ex}) / \Delta_i^{in}$. With increased intrusion step, the pore entrapment $\alpha_{en}$ can be expressed in relation to $d_i$.

### 2.3 Transport property measurement

In this paper, the transport property in saturated mortars is indicated by means of rapid chloride migration test. The non-steady-state migration coefficient $D_{RCM}$ ($\times 10^{-12}$ $m^2/s$) is calculated using the equation (2) proposed by Tang et al. [9]:

$$D_{RCM} = \frac{0.0239(237+T)L}{(U-2)t}\left(x_d - 0.0238\sqrt{\frac{(237+T)Lx_d}{U-2}}\right) \quad (2)$$

where, U is absolute value of the applied voltage (V); T represents average value of the initial and final temperatures in the anolyte solution (°C); L denotes thickness of the specimen (mm); $x_d$ indicates average value of the penetration depths (mm); t is test duration (hour).

## 3. RESULTS AND DISCUSSIONS

### 3.1 Mercury intrusion with additional extrusion-intrusion cycles

Figure 2 shows the logarithmic pore size distributions derived from intrusion steps 8-13 and step 20 for one-year cured OPC paste P5. As indicated, the maximum mercury intrusion occurs at step 8, with a critical pore diameter of 45.8 nm. From intrusion step 9 onwards, the derived pore size distribution curves for pores larger than this critical diameter (45.8 nm) are all overlapped (red line) and equal to that derived from the 2nd intrusion branch (step 20), which reveals that all the large capillary pores has already been filled with mercury after the critical pores have been intruded.

Above observation is reasonable if looking at the sketch of pore structure as indicated in Figures 1a and 1b. Accordingly, the majority large capillary pores cannot be filled with mercury when pressurization commences. Instead, increased applied pressure firstly leads to mercury intrusion into the small capillary pores. When a critical pressure is attained, corresponding to critical pore diameter ($d_{cr}$) via Washburn equation, a percolating network has been formed among small capillary pores in contact areas. Subsequently, all the large capillary pores can be connected and intruded with mercury abruptly. Figure 2 shows that the capillary pores smaller than 0.1 μm can be considered as small capillary pores.

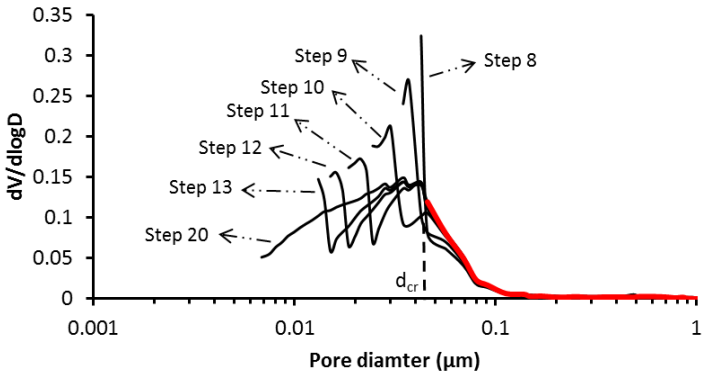


Figure 2: Logarithmic pore size distributions from mercury intrusion steps 8-13 and step 20, OPC paste P5, w/c=0.5, curing age one year.

With further pressurization, the small capillary pores smaller than $d_{cr}$ are gradually intruded with mercury at applied pressures corresponding to their pore radii. From Figure 2, the volume of each pore size smaller than $d_{cr}$ is increased with intrusion step. This unveils that all these fine pores are mutually interconnected.

The results presented in Figure 2 agree well with pore structure model shown in Figures 1a and 1b. It can be thus concluded that the pores in hydrated cement paste are not completely randomly distributed; instead their connections do impose regularities. In summary, the connections of pores with different dimensions can be classified into two groups: (i) Pores above critical diameter $d_{cr}$. These pores can make up a percolating pore network throughout the hydrated OPC paste. In accordance to pore structure model (Figures 1a and 1b), such percolating pore network includes all the large capillary pores and a certain quantity of small capillary pores. These small capillary pores mainly refer to those present in contact areas as well as in outer front of outer product zones. In addition, these small capillary pores mostly act as throat neck and connect with large capillary pores of dead-end type. (ii) Pores below critical pore diameter $d_{cr}$. They are mutually interconnected but do not have any connection with large capillary pores.

### 3.2 Pore connection in hydrated cementitious materials

In this work, the connectivity of pores with different dimensions is studied through analysing the pore entrapment $\alpha_{en}$ against penetrated pore diameter $d_i$. Lower $\alpha_{en}$ value means that the penetrated pores exhibit higher connectivity in the pore network. According to table 2, relation ($\alpha_{en}$ *vs.* $d_i$) can be obtained when $d_i$ is changing from 259 nm to 7 nm. The following paragraphs illustrate relation ($\alpha_{en}$ *vs.* $d_i$) in paste specimens made with varying microstructures.

***OPC paste***

Figure 3 plots the relation ($\alpha_{en}$ *vs.* $d_i$) in OPC pastes. The effects of curing age (Figure 3a) and w/c (Figure 3b) are studied. As can be seen, all the curves are present in similar pattern, and strong relationships are observed between $\alpha_{en}$ and $d_i$. Regardless of w/c and curing age, each curve can be categorized into two groups according to penetrated pore size above or below critical pore diameter ($d_{cr}$) in corresponding mixtures (Figure 3a), and there is an abruptly drastic drop in $\alpha_{en}$ value from capillary pore group above $d_{cr}$ to capillary pore group below $d_{cr}$. Though it should be noted that increased curing age and decreased w/c strengthen the pore entrapment, in another word, the volume fraction of dead-end pores is enlarged.

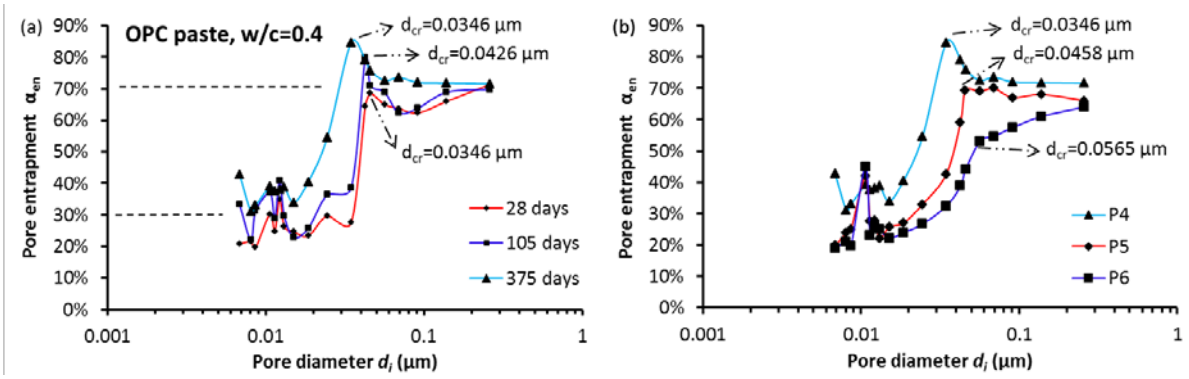


Figure 3: Relation ($\alpha_{en}$ *vs.* $d_i$) in OPC pastes: (a) w/c=0.4, curing age from 28 days to 375 days, (b) w/c=0.4, 0.5 and 0.6, curing age 375 days.

Moreover, similar small peaks are observed in all the plots at $d_i$ around 10 nm, which represent the pore connection in gel pore system and result from the mercury penetration in the inner product zones (Figure 1b). The high pore entrapments (around 70%) for pores above $d_{cr}$ manifest their poor connections in OPC pastes. Conversely, the pore entrapments are approximately 30% for pores below $d_{cr}$, which reveals that the small capillary pores in patches of OPC hydrates are highly interconnected.

***Blended cement pastes***

Figures 4a and 4b show the differences in pore entrapment $\alpha_{en}$ between neat OPC paste (P5) and blended cement pastes after curing 375 days. Note that various mixtures exhibit different critical pore diameters ($d_{cr}$) but all of which are approaching to 50 nm. Overall speaking, regardless of w/b and added blends, the pore entrapment $\alpha_{en}$ for pores above 50 nm in each plotted curve is not significantly changed and mainly lies in between 60-78% among all the mixtures. Nonetheless, the pore entrapments $\alpha_{en}$ for pores below 50 nm in all the plotted curves are tremendously varied in the range 20-82%. In particular, inclusion of various blends either FA or slag commonly results in higher pore entrapment for most pores below 50 nm.

This can be attributed to the fact that in these blended systems, much more hydrated C-S-H gels have been produced due to pozzolanic reactions; as a consequence considerable amount of small capillary pores should have been entrapped by such gels and exhibited as dead-end pores, resulting in more tortuous capillary pore network.

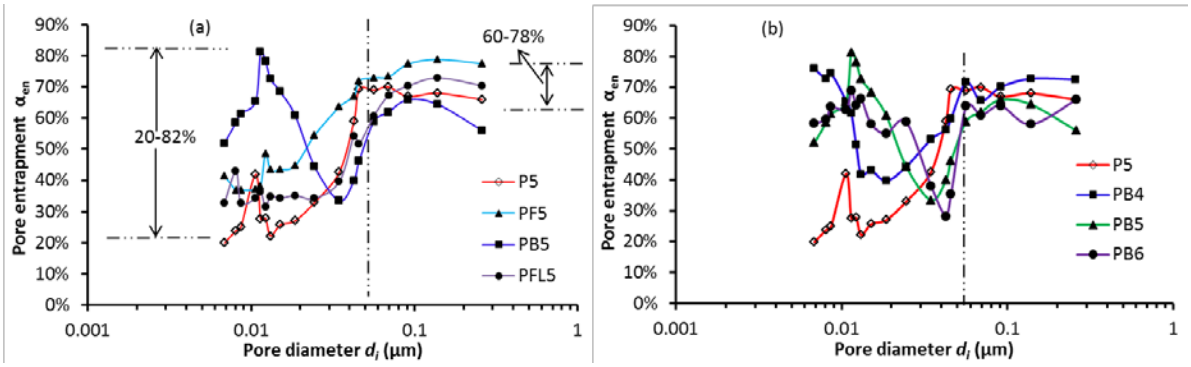


Figure 4: Relation ($\alpha_{en}$ *vs.* $d_i$) in blended cement pastes cured at 375 days.

### 3.3 Pore connectivity η (η =1-$\alpha_{en}$) and transport property ($D_{RCM}$)

Pore structure model (Figures 1a and 1b) has shown us that it is the small capillary pores (10 nm ~ 0.1 μm) within patches of outer hydration products that constitute the majority of continuous pores and govern the whole capillary percolating network, which has also been demonstrated by the mercury intrusion experimental results as presented in Figures 2 and 3. Therefore, the pore connectivity of small capillary pores should dominate mass transport in hydrated cementitious system. Figure 4 has further revealed that the pore connectivity of small capillary pores in blended cement pastes is much lower than that in neat OPC pastes.

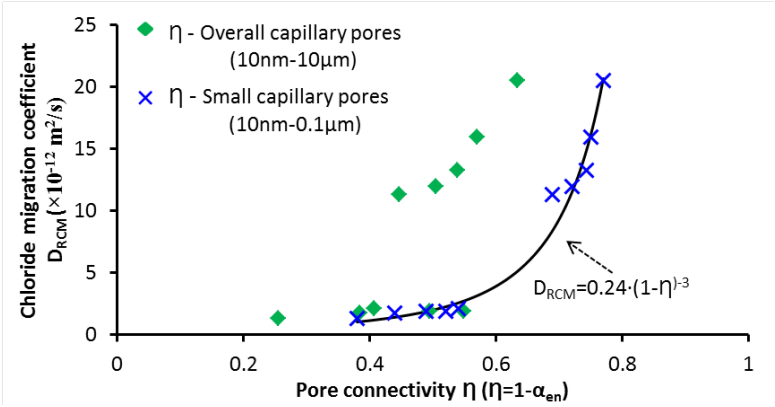


Figure 5: Chloride migration coefficient ($D_{RCM}$) against pore connectivity η for the overall capillary pores (10nm-10μm) and for small capillary pores (10nm-0.1μm) respectively.

As aforesaid in section 3.1, once critical pores ($d_{cr}$) have been intruded with mercury, the subsequent penetrated pores (i.e. 10 nm ~ $d_{cr}$) are all belonging to small capillary pores. Given the fact that the small capillary pores are formed due to similar refinement mechanism, for a simple calculation, herein the connectivity η of small capillary pores (i.e. 10 nm ~ 0.1 μm) is representatively indicated by the connectivity of pores below $d_{cr}$ (i.e. 10 nm ~ $d_{cr}$), which can be measured by mercury intrusion experiment and calculated following equation

(3). Herein, $\alpha_{en}$ is the cumulative pore entrapment in the pore size range (10 nm ~ $d_{cr}$); $V_{10}^{in}$ ($V_{d_{cr}}^{in}$) and $V_{10}^{ex}$ ($V_{d_{cr}}^{ex}$) represent cumulative intruded volume and subsequent cumulative extruded volume after mercury penetration into pores of 10 nm ($d_{cr}$).

$$\eta = 1 - \alpha_{en} = (V_{10}^{ex} - V_{d_{cr}}^{ex}) / (V_{10}^{in} - V_{d_{cr}}^{in}) \quad (3)$$

Figure 5 presents well-fitted experimental plots between chloride migration coefficient $D_{RCM}$ and pore connectivity η of small capillary pores (10 nm ~ 0.1 μm). For a comparison, the $D_{RCM}$ is also plotted against the calculated η for the overall capillary pores (10 nm ~ 0.1 μm), yet no fixed correlation can be obtained.

## 4. CONCLUSIONS

- Mercury penetration experiment with additional extrusion-intrusion cycles was carried out on a variety of hydrated cement pastes curing up to one year, whereby the small capillary pores that present within patches of hydration products and large capillary pores that represent void space left out of hydration products are distinguished. Regardless of water-binder ratio, curing age and added blends, the large capillary pores (>0.1 μm) in hydrated cement pastes are poorly connected and mostly present as dead-end pores. The small capillary pores (<0.1 μm) in OPC pastes are highly interconnected and mostly present as continuous pores. Partial replacement of OPC by blends either fly ash or slag would significantly reduce the pore connectivity of small capillary pores.
- It is suggested that the pore connectivity of small capillary pores dominates mass transport in hydrated cementitious materials under saturated condition. This has been supported by the well-fitted experimental plots in this study.

## ACKNOWLEDGEMENTS

The authors acknowledge the financial support from Chinese Scholarship Council (CSC).

## REFERENCES

[1] Stark J., 'Recent advances in the field of cement hydration and microstructure analysis', *Cem. Concr. Res.* 41 (2011) 666–678.
[2] Mindess J.S. and Young J.F., 'Concrete', (Prentice-Hall, Englewood Cliffs, NJ, 1981).
[3] Powers T.C., Brownyard T.L., 'Studies of the physical properties of hardened Portland cement paste. Part 2. Studies of water fixation', *J. Am. Concr. Inst.* 18 (3) (1946) 249–303.
[4] van Breugel K., Numerical simulation of hydration and microstructural development in hardening cement-based materials. PhD thesis (Delft University of Technology, the Netherlands, 1991)
[5] Bentz D.P., 'Fibers, percolation, and spalling of high performance concrete', *ACI Mater. J.* 97 (3) (2000) 351– 359.
[6] Navi P. and Pignat C., 'Simulation of cement hydration and the connectivity of the capillary pore space', Advanced cement-based materials. (4) (1996) 58-67.
[7] Diamond S., 'Mercury porosimetry: an in appropriate method for the measurement of pore size distributions in cement-based materials', *Cem. Concr. Res.* 30 (10 (2000) 1517-1525.
[8] Washburn, E.W., 'The dynamics of capillary flow', *Phys. Rev.*, 17 (1921) 273-283.
[9] Tang L.P. and Nilsson L.O., 'Rapid determination of the chloride diffusivity in concrete by applying an electrical field', *ACI materials journal* 89 (1) (1992) 49-53.